JMEPEG (2009) 18:878–885
DOI: 10.1007/s11665-008-9318-1

1059-9495/$19.00

Fabrication of 3-D Submicron Glass Structures by FIB

C.H. Chao, S.C. Shen, and J.R. Wu

(Submitted November 13, 2007; in revised form September 19, 2008)

The fabrication characteristic of focused ion beam (FIB) for Pyrex glass was investigated. FIB has several advantages such as high resolution, high material removal rates, low forward scattering, and direct fabrication in selective area without any etching mask. In this study, FIB-etched Pyrex glass was used for fast fabrication of 3-D submicron structures. A glass structure with 0.39 μm in width was fabricated. The experimental results in terms of limiting beam size, ion dose (ion/cm^2), and beam current are discussed. The influence of XeF_2 gas on FIB glass fabrication was investigated.

Keywords focused-ion beam, pyrex glass, submicron, XeF_2

1. Introduction

Nanotechnology has been regarded as the fourth industrial revolution and the key driver of new technology developments in the twenty-first century. Particularly, nanotemplate manufacture technology is a target of interest for the MEMS industry (Ref 1). Glass, used for anodic bonding with silicon, is a widely used substrate material, especially in the biochip fabrication (Ref 2-4). In fluidic MEMS, polymer materials have been employed widely due to their low cost. Glass is much more suitable for high temperature applications in reactive chemical environments. In optical applications, glass is a good material for its enhanced optical properties.

The most common and well-known glass micromachining method is hydrofluoric acid (HF) wet etching with etching mask of different mask materials. Etching masks can be fabricated using processes such as plasma enhanced chemical vapor deposition (PECVD) amorphous silicon layers (Ref 5), low pressure chemical vapor deposition (LPCVD) polysilicon layers (Ref 6), and anodically bonded silicon substrates (Ref 7). Moreover, the combination of mechanical machining by nanoindenter and wet etching of Pyrex glass is a maskless fabrication process to define pattern on glass. On glass surface, the 1 μm wide and 160 nm high convex structures were fabricated by HF solution etching. The 1 μm wide and 60 nm deep grooves were machined by nanoindenter with scratching velocity 10 μm/s and normal load 5 mN. The aspect ratio of the convex structure was low (∼0.16) due to the etching of the amorphous Pyrex glass (Ref 8). Dry etching is not suitable for glass machining because of its low etching rate. Deep reactive ion etching (DRIE) of Pyrex glass using sulfur hexafluoride plasma (SF6) and 20 μm thick electroplated nickel film as etch mask under conditions of low pressure (0.2 Pa) and low etching rate (∼0.6 μm/min) was reported to fabricate microstructures (Ref 9). In addition, using CHF_3 plasma with a 135 μm thick silicon wafer bonded to a Pyrex glass wafer as an etching mask, it is possible to fabricate a deep groove of 1×1 mm^2 square and 430 μm depth under conditions of low pressure and etching rate (∼0.5 μm/min) (Ref 10). Powder blasting was used in glass machining but the quality of the etched surface was not suitable for biochip applications (Ref 11, 12). For this reason, many researchers studied new methods for the micro/nanomachining of glass structures.

The FIB technique was mainly developed during the period 1970-1980 (Ref 13). This technology enables precise cutting, selective deposition, enhanced etching, and end point detection. It has many potential applications such as prototype modification, micromachining (Ref 14), failure analysis by local cross sectioning (Ref 15), transmission electron microscopy (TEM) sample preparation (Ref 16, 17). FIB has several advantages such as high resolution and material removal rates, low forward scattering, direct fabrication in selective area without any etch mask. 3-D structure depth gradation of order of 10 nm was machined on spin-on-glass (SOG) resists by FIB, but the aspect ratio was small ($\ll$1) (Ref 18). Optical elements can be microfabricated on selective areas of glass by FIB etching, Electron beam lithography (EBL), or laser beam writing (LBW). They are all useful for rapid prototyping of optical elements with continuous relief and profile with an accuracy smaller than 100 nm. But EBL and LBW need an extra exposure to define the pattern, which leads to higher writing time and cost than FIB etching (Ref 19).

Since the applications of glass microdevices are expanded, the need of a precise and flexible micro/nanostructuring technique for glass has increased. Fabrication of microscale and nanoscale structured glass can be carried out by various methods such as wet/dry etching, laser machining, FIB, powder blasting, and mold replication technique. Among these, FIB offers a high flexibility in the working shapes and dimensions (a scale ranging from a few tens of nanometers to hundreds of micrometers), and a variety of material selectivity. In addition, FIB is a very powerful maskless technique for both micro- and nanostructuring. It can be applied to micro/nanoscale fabrication. In addition, FIB has several advantages such as high

C.H. Chao and **J.R. Wu**, Department of Mechanical and Electro-Mechanical Engineering, and Center for Nanoscience & Nanotechnology, National Sun Yat-Sen University, Kaoshiung 804, Taiwan; and **S.C. Shen**, Department of Systems and Naval Mechatronic Engineering, National Cheng Kung University, Tainan 701, Taiwan. Contact e-mail: scshen@mail.ncku.edu.tw.

sensitivity and low forward scattering. Moreover, FIB machines now have been improved to give finer beam diameter with good stability of ion source operation. Therefore, FIB is seen as a promising technology for rapid fabrication. Laser-assisted direct imprint shows great potential to fabricate micro/nanoscale structure on silicon wafer (Ref 20). However, it needs a mold that is made of ultraviolet transparent material such as quartz. Therefore, fabrication of quartz mold with submicron/nanoscale structures becomes a critical technology for imprint (Ref 21, 22); however, there has been only little study on FIB processing quartz material.

This paper reports on the fabrication of a 3-D template and investigations of the characteristics of the FIB process on Pyrex glass. In this study, micro/submicron-machining on Pyrex glass is realized using FIB to fabricate a 3-D submicron structures. The factors influencing the manufacturing process, which include ion dose, beam size, and beam current, are analyzed. The influence of XeF_2 gas on FIB glass fabrication is investigated.

2. Experimental Apparatus and Procedures

In this study, 4-inch Pyrex glass wafers with 500 μm in thickness were prepared for the FIB process. First, the wafer was cleaned using DI water and acetone in the ultrasonic bath and then baked for 10 min in the hot plate at 60 °C. The insulating property of glass leads to ion beam scattering and accumulation on the glass surface. A thin Chromium (Cr) film with 7.5 nm thickness was deposited on the wafer as a conductive layer by thermal evaporation at a working pressure of 5×10^{-6} Torr and a current of 100 A. The Pyrex glass wafer was cut into samples of 2×2 cm^2 in area for FIB process.

The patterning of Pyrex glass was carried out using a dual-beam FIB machine (SMI3050SE purchased from SII Nano-Technology Inc. in Japan) with an ion source of liquid gallium, integrated with a scanning electron microscope (SEM). This combination was to avoid having to use multiple tools for sample preparation and imaging. The FIB instrument consists of a vacuum system and chamber, a liquid metal ion source, an ion column, a sample stage, detectors, gas delivery system, and a computer. Table 1 shows the equipment capability of the dual-beam FIB. The highest accelerating voltage is 30 keV. The beam conditions were set at "Fine" and "UFine" modes, respectively. Table 2 shows the detailed beam condition for the FIB machining. The pressures in the chamber and ion column are 5.7×10^{-5} Pa and 4.6×10^{-6} Pa, respectively. Pattern definition is done by SMI3050SE software. The test patterns in this study are 3-D pyramids. The process flow is schematically shown in Fig. 1. Through the user interface, the fabrication parameters such as beam condition, dwell time, depth, overlap percentage, gas species, and material are set. The depth correlates well with ion dose. The dwell time means the time the ion beam stays in each pixel. The overlap percentage is the ratio of the separation of two pixels divided by the size of the ion beam. The scan consists of stepping irradiation with the dwell time of 100 μs and the overlap percentage is 0%. The gas-assisted chemically enhanced FIB micromachining (CE-FIBM) provides chemical reaction with the material surface during machining process. CE-FIBM has the advantages of material removal rate enhancement and material selectivity enhancement. Fabricated submicron pyramids were directly observed by SEM.

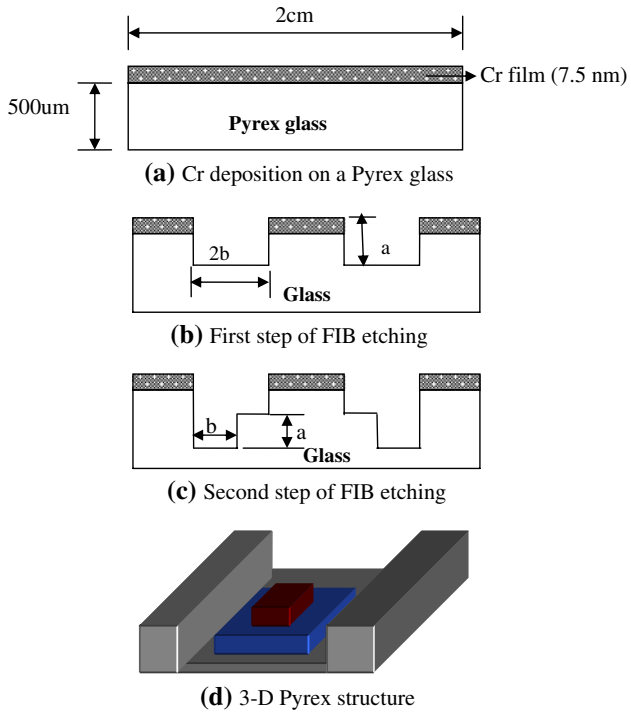

Fig. 1 Schematic of FIB etching process of Pyrex glass

Table 1 Equipment capability of dual-beam FIB

Type	SMI3050SE/FIB-SEM hybrid system
Functions	(1) Precisional cutting
	(2) Selective deposition
	(3) Enhanced etching/Selective etching
	(4) End point detection
Main specifications	
FIB	Ion source: Liquid metallic gallium
	Secondary electron image resolution: 4 nm/30 kV
	Ion beam current range: 0.15 pA to 20 nA
	Acceleration voltage: 5-30 kV, 5 kV step
SEM	Secondary electron image resolution: 5 nm/1 kV,
	Acceleration voltage: 0.5-15 kV
Sample stage	5 Axis motor operation: XY feed-back control
	Stage repeatability: ±2 um(X,Y)
	Operation range: X = 0 to 55 mm
	Y = 0 to 50 mm
	Z = 0 to 10 mm
	T = 4 to 60 degrees
	Maximum specimen size: 50 mm^2, Thickness: 12 mm

Table 2 Etching condition of FIB machining

Acceleration voltage, kV	30	
Dwell time, μs	100	
Overlap	0%	
Beam condition	Fine	UFine
Ion beam current, pA	267.6	104.5
Beam size, nm	38	22

3. Experimental Results and Discussion

The experimental results of this study are discussed in three categories. First, to investigate the relationship between the beam conditions, ion dose, etching depth, and broadening effect on the profile of the pattern, different ion doses and beam conditions have been conducted for FIB fabrication of Pyrex glass. The relationships between these parameters are depicted in Fig. 2(a) and (b). The depth variation caused by beam condition is small, but broadening width effect variation is significant as shown in Fig. 2(a). Figure 2(b) shows that the etching depth of Pyrex glass increases linearly with ion dose. When the ion dose increases from 100×10^{15} to 540×10^{15} ion/cm^2, the etched depth increases from 26 to 130 nm. At a low dose of 100×10^{15} ion/cm^2, the broadening widths for "Fine" and "UFine" modes are 240 and 129 nm, respectively. With increase in dose up to 540×10^{15} ion/cm^2, the broadening width variation of UFine mode is small, but Fine mode increases linearly. This suggests that the etching depth is not affected by the beam conditions. The broadening width of Pyrex glass increases with ion dose. The broadening width of "UFine" mode is smaller than that of "Fine" mode under the same fabrication condition. The results revealed a correlation between the beam condition selection and broadening width effect. It was clear that the structure width was dependent on the beam conditions. A smaller beam size and current result in a better process quality.

Second, a further experiment was conducted on the effect of FIB on 3-D submicron structures fabrication. The schematic illustration of the 3-D pyramids is shown in Fig. 1. Several

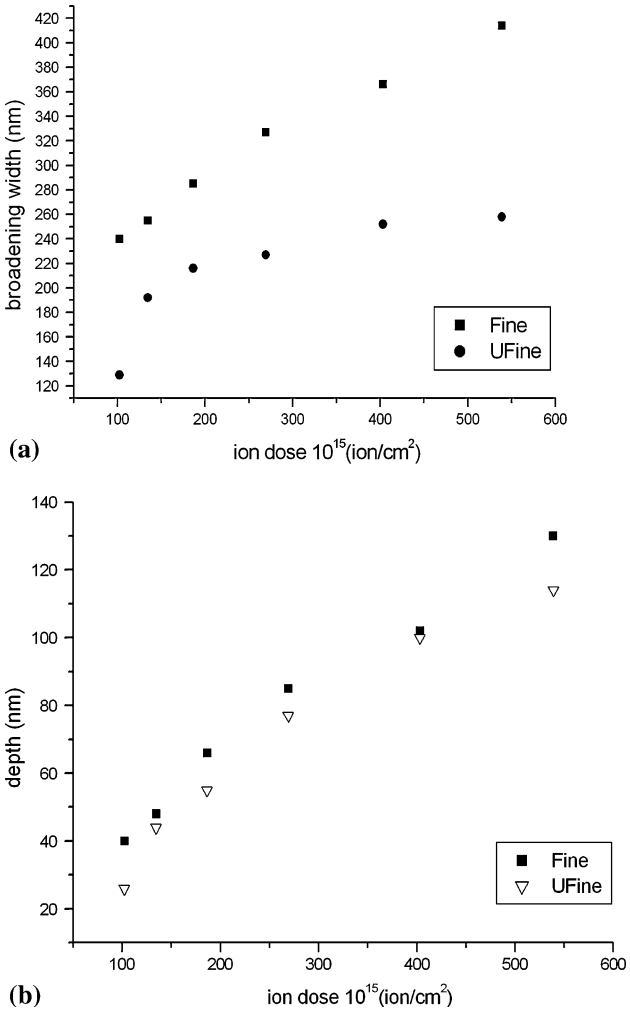

Fig. 2 Ion dose versus (a) broadening effect and (b) depth of Pyrex glass for different beam conditions

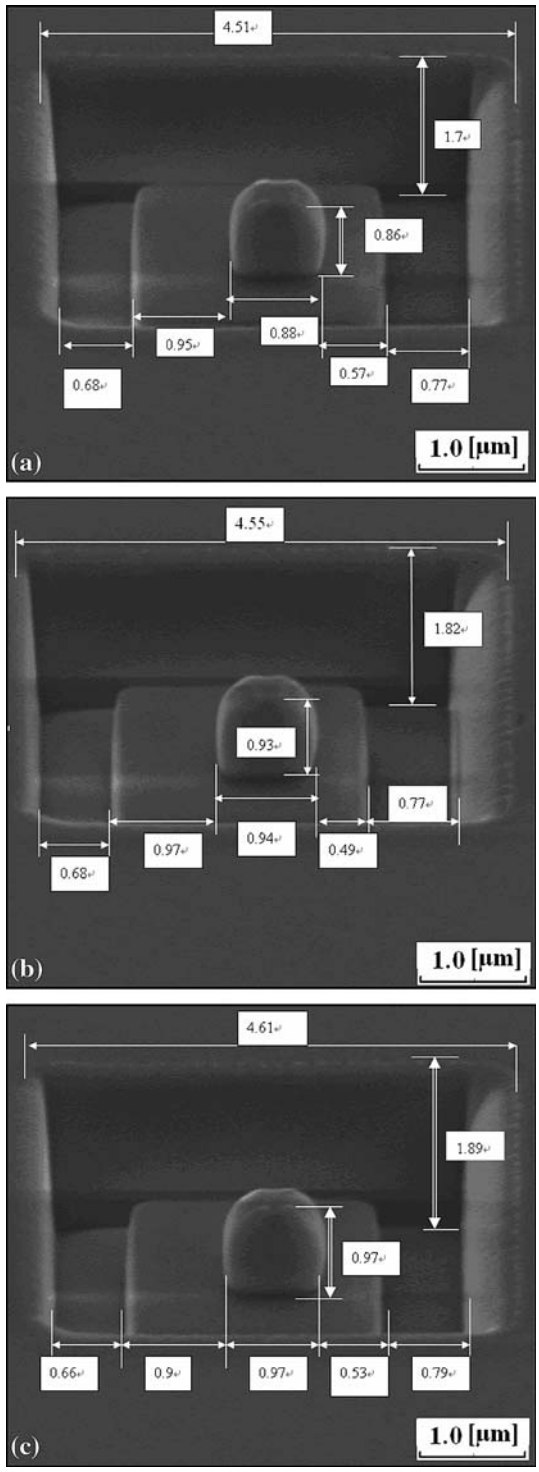

Fig. 3 Typical SEM image of depth gradations of (a) $a = 0.85$, (b) $a = 0.9$, and (c) $a = 0.95$. The designed line-width is 0.8 μm

step-shape pyramids were fabricated. Figure 3 shows the image of pyramids fabricated with depths of 0.85, 0.9, and 0.95 μm at a designed line-width of 0.8 μm and an etching area of 4 by 4 μm. Under the same etching parameters (i.e., dwell time, acceleration voltage, overlap percentage), the beam condition for the first step and second step is "Fine" and "UFine", respectively. As the etching depth increases, the width of tapered side wall becomes larger, and increases from 4.51 to 4.61 μm. Figure 4 shows the etching rate for different ion doses with a designed line-width of 0.8 μm. The etching rate for the first step and second step is 47.74×10^{-4} and 26.33×10^{-4} μm/s, respectively. Figure 5 shows the etching depth with respect to different ion doses. The numerical results show that the material removal rate is approximately 3.7×10^{-11} μm^3/ion. The etching depth of Pyrex glass increases linearly with ion dose. Figure 6 shows the etching depth as a function of processing time. The etching depth of Pyrex glass increases linearly with ion dose. It is apparent from the figures that the etching depth of Pyrex glass increases linearly with ion dose and processing time. Figure 7 shows the image of pyramids fabricated with designed depths of 0.85, 0.9, and 0.95 μm at a designed line-width of 0.85 μm and an etching area of 4.25 by 4.25 μm. The beam condition for the first step and second step is "Fine" and "UFine" mode, respectively, in the FIB process. With increase in etching depth, the width of tapered side wall increases from 4.71 to 4.8 μm. Figure 8 shows the etching rate for different ion doses and processing procedure at a designed line-width of 0.85 μm. The etching rate of different ion doses is similar. The etching rate for the first step and second step is 42.44×10^{-4} and 24.3×10^{-4} μm/s, respectively. Figure 9 shows the experimental image of pyramids fabricated with designed depths of 0.85, 0.9, and 0.95 μm at a designed line-width of 0.9 μm and an etching area of 6 by 6 μm. The beam condition is "UFine" mode in the FIB process. As the etching depth is increased, the broadening width increases from 6.47 to 6.51 μm. The tapered angle of the wall approaches 90° using the small beam condition. Figure 10 shows the etching rate for different ion doses and machining procedure at a designed line-width of 0.9 μm. The etching rate of different ion doses is similar. The etching rate for the first step and second step is 9.8×10^{-4} and 15.17×10^{-4} μm/s, respectively. All of the above-mentioned SEM images indicate that the designed depth resembles the experimental depth well. The scattering and accumulation of ion beam lead to a width irregular of 3-D pyramid.

These data are estimated from the SEM photographs. The geometry of the multilevel structure with steep step is difficult to measure by AFM (atomic force microscope), owing to the restriction of the motion of the AFM's probe. Therefore, error

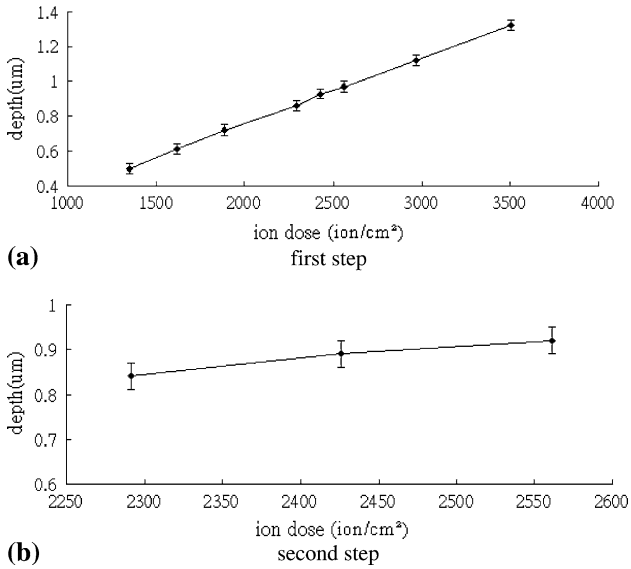

Fig. 5 Ion dose versus depth for machining procedure. The designed line-width is 0.8 μm

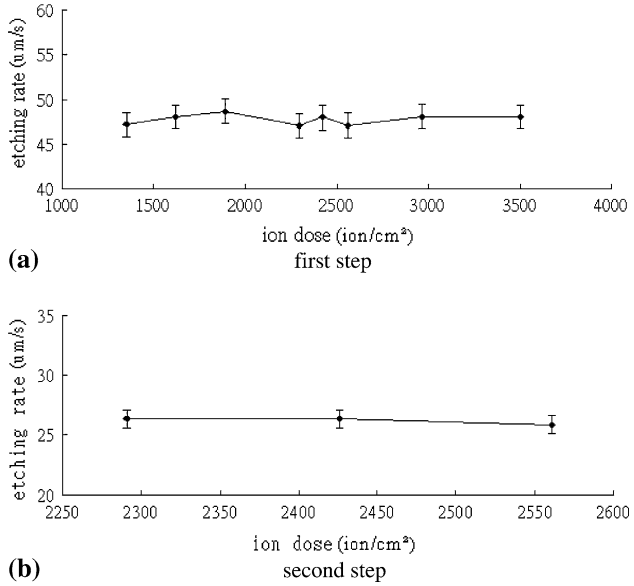

Fig. 4 Ion dose versus etching rate for machining procedure. The designed line-width is 0.8 μm

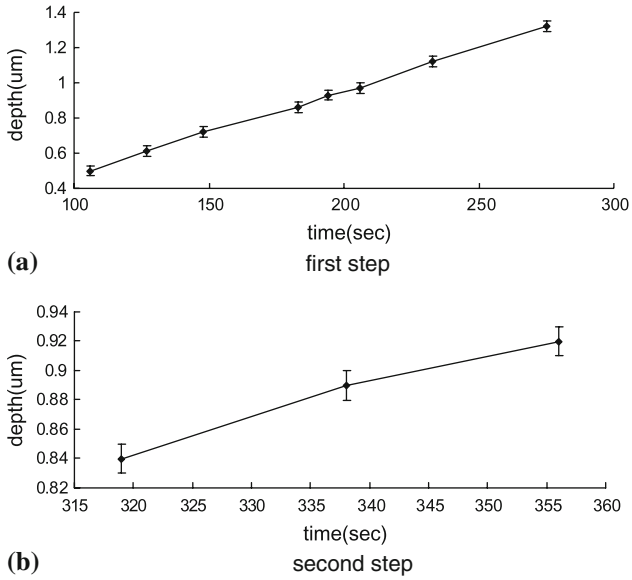

Fig. 6 Ion dose versus time for machining procedure. The designed line-width is 0.8 μm

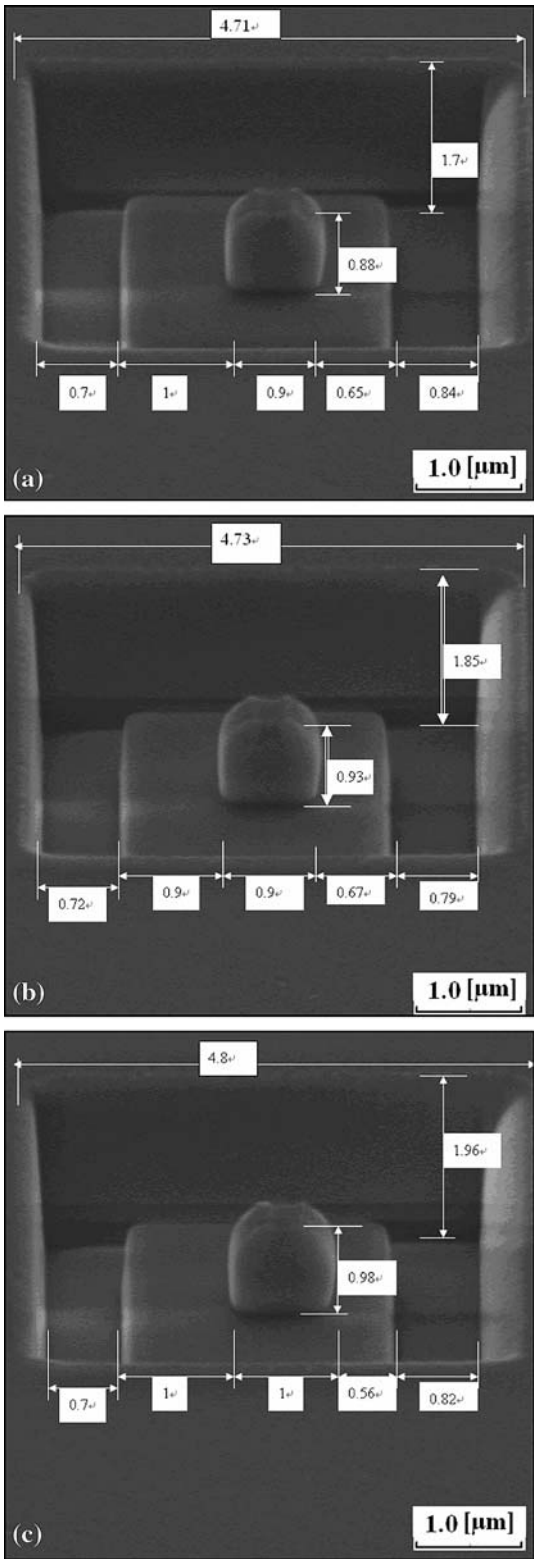

Fig. 7 Typical SEM images of (a) $a = 0.85$, (b) $a = 0.9$, and (c) $a = 0.95$. The designed line-width is 0.85 μm

bars have been added to the figure. In this study, three different values of ion doses were designed, which have drastic difference in the values. By doing this, an obvious trend of the effect of the ion dose can be observed.

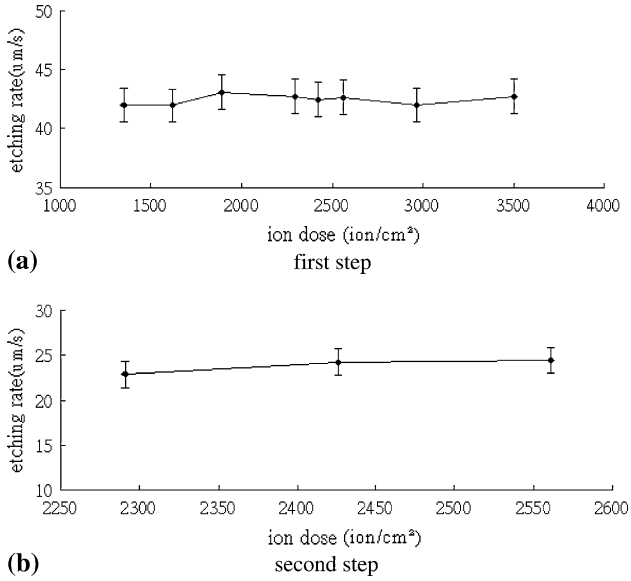

Fig. 8 Ion dose versus etching rate of Pyrex glass for machining procedure. The designed line-width is 0.85 μm

The authors expected 5(b) and 6(b) to be linear but did not expect 4(b), 8(b), and 10(b) to be linear. The material removal rate was approximately 3.7×10^{-11} μm^3/ion so that the etching rate does not change as ion dose increases. In addition, the effect of re-deposition can cause the depth to be different from the designed depth.

The presence of XeF_2 during FIB micromachining for FIB increases the removal rate of SiO_2. Table 3 and 4 show the etching conditions and processing time for the CE-FIBM under the same designed width (b = 0.9 μm) and the different designed depths. They are summarized in Table 3 and 4. The processing time of CE-FIBM is close to the FIB under the same machining condition. According to the processing time, the designed depth of 1.8 μm is smaller than the designed depth of 0.85 μm. It may be concluded at this point that the smaller beam size and current result in a longer machining time. Figures 11(a) and 12(a) show the SEM images of the pyramid fabricated by FIB process, and the SEM photographs of the pyramid by CE-FIB processes with XeF_2 gas are illustrated in Fig. 11(b) and 12(b). Figures 11(a) and (b) shows that the maximum etching depth is 2.6 and 0.9 μm, respectively. The enhanced etching resolution of Pyrex glass is 2.6 μm in depth and 0.9 μm in depth for XeF_2 CE-FIBM. Figure 11(a) shows that the surface is not completely flat. Figure 12(b) shows an image of the pyramid fabricated with minimum etched width 0.39 μm at an etching depth of 1.97 μm. When etching depth was increased by CE-FIB, the top structure tapered off to a point by the subsequent etching. The surface roughness becomes larger. This is clear from Fig. 12(a). From these figures, the etching depth of the structure was significantly enhanced when the pyramids were fabricated by CE-FIBM processes. This feature is most likely attributed to the formation of $SiF_x^+ (x = 0\text{-}4)$ and $SiOF_y^+ (y = 0\text{-}2)$ from the chemical reaction between XeF_2 and SiO_2 (Ref 23). The material removal rate is approximately 2.16×10^{-10} μm^3/ion by CE-FIB processes with XeF_2 gas. It is worth noticing that the surface profile of these structures by FIB was found to be better than that by CE-FIBM.

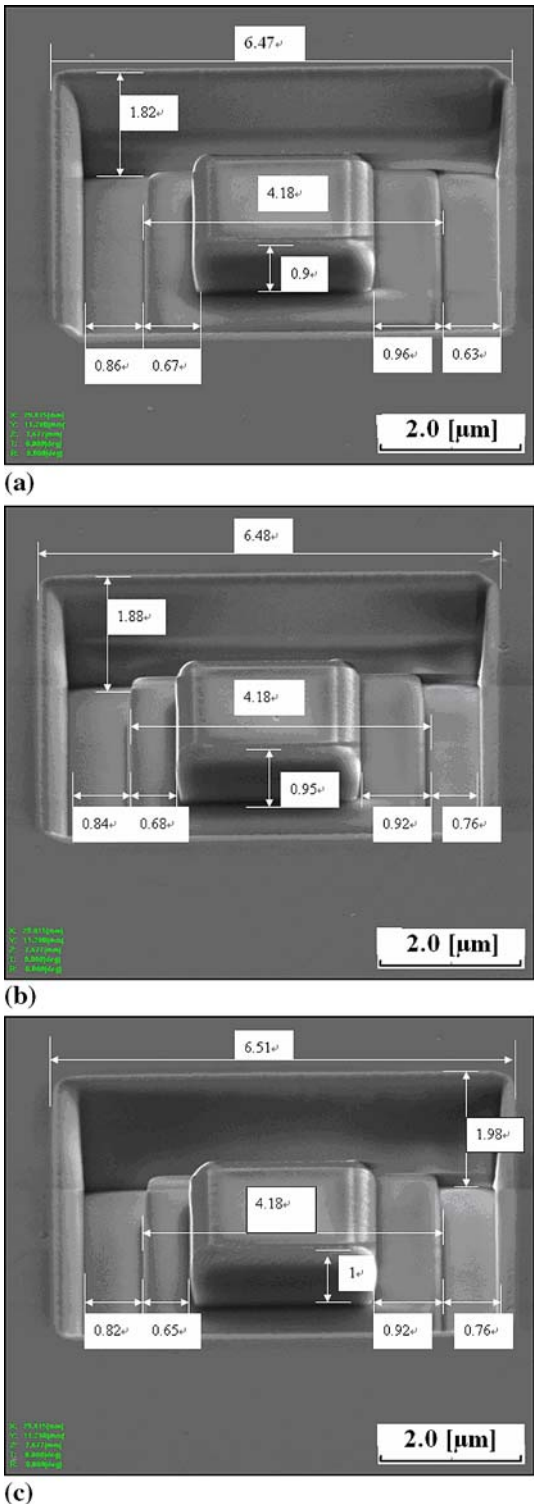

Fig. 9 Typical SEM images of (a) $a = 0.85$, (b) $a = 0.9$, and (c) $a = 0.95$. The milled area and designed depth are 6×6 μm and 0.9 μm, respectively

This simple multilevel structure was fabricated by FIB to find out the working characteristics in 3-D structures. By doing this, more complicated structures such as Fresnel lens and diffraction optical elements can be manufactured. FIB process offers a high flexibility in the working shapes ranging from a few tens of nanometers to hundreds of micrometers. These characteristics allow nano- and microstructures to be fabricated directly on Pyrex glass. To fabricate 3-D structures by FIB, some working parameters such as beam size, ion dose (ion/cm^2), and beam current were investigated. The results show that the etching depth increases linearly with ion dose and working time.

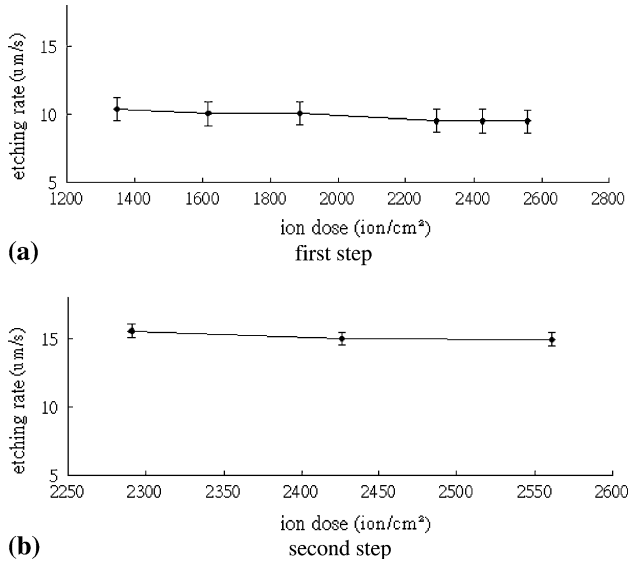

Fig. 10 Ion dose versus etching rate of Pyrex glass for machining procedure. The designed line-width is 0.9 μm

Table 3 Etching conditions and machining time of CE-FIBM under the designed depth of 0.85 μm

Beam condition	Fin	F.O.V	40
Beam angle	90	Voltage, keV	30
Dwell time, μs	100	Current, pA	267.6
Dose × 10^{15}, ion/cm^2	4851.752		
GAE-FIBM machining time, M:S	First	12:47	
	Second	7:55	
FIB machining time, M:S	First	13:08	
	Second	8:08	

Table 4 Etching conditions and machining time of CE-FIBM under the designed depth of 1.8 μm

Beam condition	UFine	F.O.V	40
Beam angle	90	Voltage, keV	30
Dwell time, μs	100	Current, pA	109.9
Dose × 10^{15}, ion/cm^2	2291.105		
CE-FIBM machining time, M:S	First	15:24	
	Second	9:32	
FIB machining time, M:S	First	15:46	
	Second	9:45	

4. Conclusions

The fabrication characteristics of FIB for Pyrex glass were investigated. A glass structure with 0.39 μm in width was

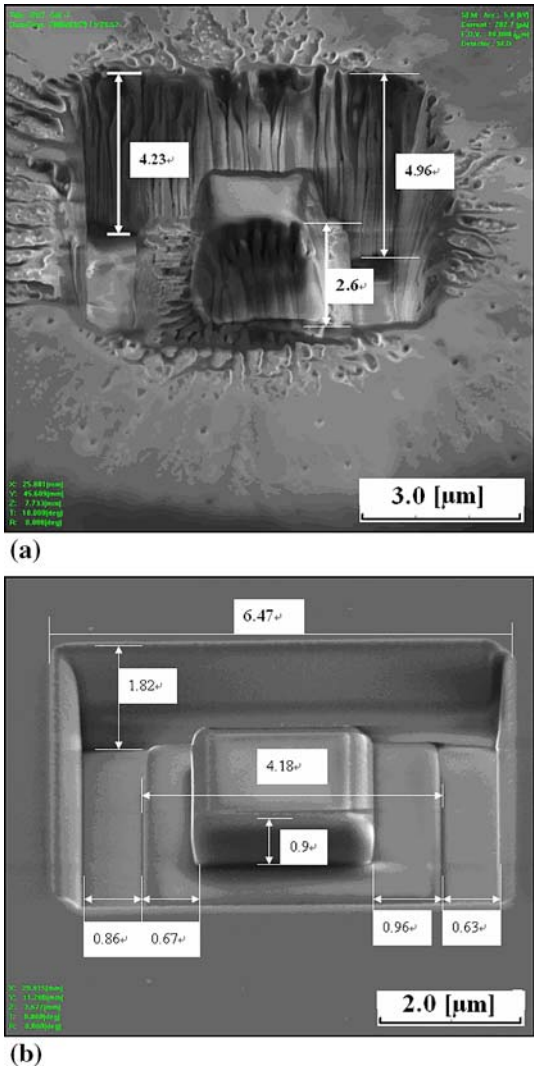

Fig. 11 SEM images of (a) CE-FIBM with XeF_2 and (b) FIBM pattern milled in Pyrex glass. The designed depth and line-width are 0.8 and 0.9 μm, respectively

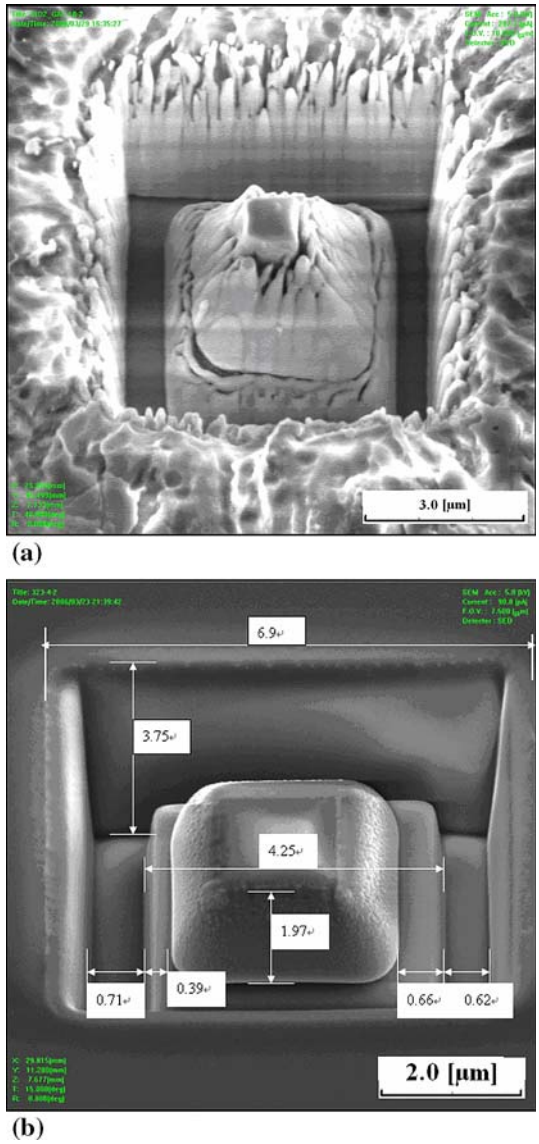

Fig. 12 SEM images of (a) CE-FIBM with XeF_2 and (b) FIBM pattern milled in Pyrex glass. The designed depth and line-width are 1.8 and 0.9 μm, respectively

fabricated. With a designed line-width of 0.8 μm, the etching rate for the first step and second step is 47.74×10^{-4} and 26.33×10^{-4} μm/s, respectively. A simple multilevel structure by FIB is designed and processed to find out the working characteristics. By doing this, more complicated structures such as Fresnel lens and diffraction optical elements can be fabricated. The etching depth of Pyrex glass increases linearly with ion dose. The results revealed a correlation between the beam condition selection and broadening width effect. It was clear that the structure width was dependent on the beam conditions. A smaller beam size and current result in a better process quality. The presence of XeF_2 during micromachining for FIB increases the removal rate of SiO_2. The enhanced etching resolution of Pyrex glass is 2.6 μm in depth and 0.9 μm in depth, for XeF_2 CE-FIBM. The material removal rate is approximately 2.16×10^{-10} μm^3/ion by CE-FIB processes with XeF_2 gas. It is worth noticing that the surface profile of these structures by FIB was found to be better than that by CE-FIBM.

Acknowledgments

The authors would like to thank the Center for Nanoscience & Nanotechnology, National Sun Yat-Sen University, Kaoshiung, Taiwan, for equipment access and technical support, and National Science Council (NSC) for their financial supports to the project (Grant numbers: NSC97-2218-E-006-009, NSC94-2213-E-110-043, NSC 94-2212-E110-015, NSC94-2622-E-110-017-CC3, and NSC95-2221-E-110-011-). The authors would like to thank the Center for Micro/Nano Technology Research, National Cheng Kung University, Tainan, Taiwan, for equipment access and technical support as well.

References

1. X.C. Shan, R. Maeda, and Y. Murakoshi, Development of a Micro Hot Embossing Process for Fabricating Micro-optical Devices, *Proc. SPIE*, 2002, **4936**, p 67–75

2. C.S. Effenhauser, A. Manz, and H.M. Widmer, Glass Chips for High-speed Capillary Electrophoresis Separations with Submicrometer Plate Heights, *Anal. Chem.*, 1993, **65**, p 652637–652642
3. Z.H. Fan and D.J. Harrison, Micromachining of Capillary Electrophoresis Injectors and Separators on Glass Chips and Evaluation of Flow at Capillary Intersections, *Anal. Chem.*, 1994, **66**, p 177–184
4. P.C. Simpson, A.T. Woolley, and R.A. Mathies, Micro-fabrication Technology for the Production of Capillary Array Electrophoresis Chips, *Biomed. Microdevices*, 1998, **1**, p 7–25
5. C. Iliescu, J. Miaob, and F.E.H. Tay, Optimization of an Amorphous Silicon Mask PECVD Process for Deep Wet Etching of Pyrex Glass, *Surf. Coat. Technol.*, 2005, **192**, p 43–47
6. M.A. Gretillat, et al., A New Fabrication Method for Borosilicate Glass Capillary Tubes with Lateral Inlets and Outlets, *Sens. Actuators A*, 1997, **60**, p 219–222
7. T. Croman, P. Enokson, and G. Stemme, Deep Wet Etching of Borosilicate Glass Using an Anodically Bonded Silicon Substrate as Mask, *J. Micromech. Microeng.*, 1998, **8**, p 84–87
8. S.W. Youn and C.G. Kang, Maskless Pattern Fabrication on Pyrex 7740 Glass Surface by Using Nano-scratch with HF Wet Etching, *Scripta Mater.*, 2005, **52**, p 117–121
9. X. Li, T. Abe, Y. Liu, and M. Esashi, Deep Reactive Ion Etching of Pyrex Glass Using SF6 Plasma, *Sens. Actuators A*, 2001, **87**, p 139–145
10. T. Akashil, Y. Yoshimura, and S. Higashiyama, Deep Reactive Ion Etching of Pyrex Glass Using a Bonded Silicon Wafer as an Etching Mask, in *Micro Electro Mechanical Systems, 18th IEEE International Conference*, 2005, p 520–523
11. E. Belloy, et al., The Introduction of Powder Blasting for Sensor and Microsystem Applications, *Sens. Actuators A*, 2000, **84**, p 330–337
12. P.S. Slikkerveer, P.C.P. Bouten, and F.C.M. de Hass, High Quality Mechanical Etching of Brittle Materials by Powder Blasting, *Sens. Actuators A*, 2000, **85**, p 296–303
13. J. Melngailis, Critical Review: Focused Ion Beam Technology and Applications, *J. Vac. Sci. Technol. B*, 1987, **5**, p 469–495
14. T. Ishitani, T. Ohnishi, Y. Madakoro, and Y. Kawanami, Focused-ion-beam 'Cutter' and 'Attacher' for Micromachining and Device Transplantation, *J. Vac. Sci. Technol. B*, 1991, **9**, p 2633–2637
15. E.C.G. Kirk, et al., Scanning Ion Microscopy and Microsectioning of Electron Beam Recrystallized Silicon on Insulator Devices, *J. Vac. Sci. Technol. B*, 1988, **6**, p 1940–1943
16. H. Ryssel, and I. Ruge, *Ion Implantation*, Wiley, New York, 1986
17. R.J. Young, E.C.G. Kirk, D.A. Williams, and H. Ahmed, Fabrication of Planar and Cross-sectional TEM Specimens Using a Focused Ion Beam, *Mater. Res. Soc. Symp.*, 1990, **199**, p 205–216
18. J. Taniguchi, K. Koga, Y. Kogo, and I. Miyamoto, Rapid and Three-dimensional Nanoimprint Template Fabrication Technology Using Focused Ion Beam Lithography, *Microelectron. Eng.*, 2006, **83**, p 940–942
19. F. Yongqi and N.K.A. Bryan, Focused Ion Beam Technique: Features Compared with Electron Beam Lithography and Laser Direct Writing for Fabrication of Optical Elements with Continuous Relief, in *Proceeding of SMA Symposium*, 2004
20. C.H. Chen, C.P. Liu, Y.C. Lee, F.B. Hsiao, C.Y. Chiu, M.H. Chung, and M.H. Chiang, IR-laser Assisted Micro/Nano-imprinting, *J. Micromech. Microeng.*, 2006, **16**, p 1463–1467
21. W. Li, S. Dimov, and G. Lale, Focused-ion-beam Direct Structuring of Fused Silica for Fabrication of Nano-imprinting Templates, *J. Microelectron. Eng.*, 2007, **84**, p 829–832
22. W. Li, G. Lalev, S. Dimov, H. Zhao, and D.T. Pham, A Study of Fused Silica Micro/Nano Patterning by Focused-ion-beam, *J. Appl. Surf. Sci.*, 2007, **253**, p 3608–3614
23. D.J. Oostra, A. Haring, and A.E. de Viries, Sputtering of SiO_2 in a XeF_2 and in a Cl_2 Atmosphere, *J. Vac. Sci. Technol.*, 1986, **6**, p 1278–1282